

The Jellium Edge and the Size Effect of the Chemical Potential and Surface Energy in Metal Slabs

Kazuhiko Seki

Nanomaterials Research Institute(NMRI),

National Institute of Advanced Industrial Science and Technology (AIST)

AIST Tsukuba Central 5, Higashi 1-1-1,

Tsukuba, Ibaraki, Japan, 305-8565, Japan

Abstract

Although free electron models have been established in order to capture the essential physics of interfacial and bulk properties in metals, some issues still remain regarding the application of free electron models to thin metal films. One of the issues relates to whether the geometric edge coincides with the potential edge in order to satisfy the charge neutrality condition when the potential profile is modeled as a rectangular potential well. We show that they coincide by rigorously taking into account the quantization effect arising from electron confinement in a thin metal slab. As a result, the overall behaviors of the chemical potential and surface energy show an increasing trend by decreasing the thickness of the slab. The chemical potential and surface energy show an oscillatory thickness dependence by further taking into account the discreteness of the total number of free electrons.

I. INTRODUCTION

Understanding quantum effects in nano-structured metals is important for developing nano-devices. Although free electron models have been used to capture the essential physics of interfacial and bulk properties in metals, [1, 2] free electron models for thin metal films have not yet been fully investigated. In thin metal films, the separation of quantum states and maximum states occupied by electrons depend on the film thickness and should be evaluated with care. One of the issues in free electron models for thin metal films relates to whether the geometric edge coincides with the potential edge in order to satisfy the charge neutrality condition when the potential profile is modeled as a rectangular potential well. Such details in this model affect the quantum effect in thin metal films. [3–6]

It is necessary to consider the background positive charge and electron density to correctly determine the electrostatic potential in metals. [2, 4, 7] The simplest model is the so-called jellium model, wherein the background positive charge is expressed as a uniform profile in the bulk of the metal sample and is sharply terminated at the surface. The cut-off edge is called the jellium edge or the geometric edge. The jellium edge is determined by imposing the charge neutrality condition, where the electron density is calculated quantum mechanically. It has been frequently stated that the jellium edge differs from the potential edge of the rectangular potential of free electrons, and others have concluded that the jellium edge and potential edge are shifted relative to each other. [3–11] On the other hand, the shift in the jellium edge away from the potential edge is not considered when calculating the chemical potential of metal films in some cases. [12–16] It has been argued whether or not the jellium edge is different from the potential surface. [3–5] In this manuscript, we scrutinize whether the jellium edge coincides with or differs from the potential edge of the rectangular potential for free electrons.

If the Fermi sphere is considered in the ground state (at temperature $T = 0$ K), the number of free electrons in the volume L^3 is expressed by [1]

$$N = 2 \frac{(4\pi/3)K_F^3}{(2\pi/L)^3}. \quad (1)$$

When the number of positive charges from ions is equal to the number of free electrons, the average density of positive charge is

$$\rho = \frac{N}{L^3} = \frac{K_F^3}{3\pi^2}, \quad (2)$$

where K_F denotes the bulk Fermi wave vector. The average positive charge density given by Eq. (2) is a consequence of the Sommerfeld model for free electrons in an infinite box potential. For the infinite barrier model, the number of positive charges increases as L^3 in such a way that N/L^3 approaches a constant value given by Eq. (2).

A free electron model of a finite width was introduced by imposing the Born-von Karman periodic boundary condition in the x and y directions, as well as a fixed boundary condition at $z = L_z$ without taking the thermodynamic limit. [7] The electron density profile along the z -direction shows oscillation with a wavelength given by π/K_F , called Friedel oscillations. [4] Friedel oscillations will be discussed later for some particular cases.

On the basis of the electron density, the jellium edge is obtained by applying the charge neutrality condition, where the average positive charge density should be correctly evaluated. In this paper, we rigorously evaluate the average positive charge density by taking into account the quantum effect arising from the finite width of the metal slab. By using the charge neutrality condition together with the rigorous results regarding the average positive charge density and the electron density profile, we show that the jellium edge coincides with the potential edge. On this basis, we study the size dependence of the chemical potential and the surface energy due to quantum confinement of free electrons in a slab.

II. THEORY

We consider a slab of finite thickness L_z in the z direction. The slab is extended infinitely in the other directions and, the Born-von Karman periodic boundary condition is imposed along the x and y directions with characteristic lengths L_x and L_y , respectively. For simplicity, we first consider the case where the potential is zero at $0 \leq z \leq L_z$ and is infinitely large at $z = 0$ and $z = L_z$. The wave function inside the slab is expressed as [4, 8]

$$\psi_k(x, y, z) = \sqrt{\frac{2}{L_x L_y L_z}} \exp[i(k_x x + k_y y)] \sin(k_z z), \quad (3)$$

where the components of the wave vectors are given by

$$k_x = \pm \frac{2\pi}{L_x} n_x, k_y = \pm \frac{2\pi}{L_y} n_y, n_{x,y} = 0, 1, 2, \dots \quad (4)$$

$$k_z = \frac{\pi}{L_z} n_z, n_z = 1, 2, 3, \dots \quad (5)$$

In the ground state (at temperature $T = 0$ K), n_x , n_y , and n_z satisfy $\hbar^2(k_x^2 + k_y^2 + k_z^2)/(2m) \leq \hbar^2 k_F^2/(2m)$, where m and \hbar are the electron mass and the Planck constant divided by 2π , respectively. k_F indicates the Fermi wave vector, *i.e.*, the largest wave vector occupied by electrons in the ground state. As shown later, k_F depends on the thickness L_z and should be distinguished from the bulk Fermi wave vector denoted by K_F except when the limit of $L_z \rightarrow \infty$ is taken.

The number of allowed values for k_x and k_y for a certain value of k_z is given by

$$\frac{L_x L_y}{(2\pi)^2} \pi (k_F^2 - k_z^2) = \frac{1}{4\pi} L_x L_y (k_F^2 - k_z^2). \quad (6)$$

The electron density profile in the ground state is obtained as [8, 17]

$$n_e(z) = 2 \frac{1}{4\pi} L_x L_y \sum_{n_z=1}^{n_{Fz}} (k_F^2 - k_z^2) |\psi_k(x, y, z)|^2 \quad (7)$$

$$= \frac{1}{2\pi L_z} \sum_{n_z=1}^{n_{Fz}} (k_F^2 - k_z^2) [1 - \cos(2k_z z)], \quad (8)$$

where spin multiplicity is included. In Eq. (8), n_{Fz} is the quantum number for the highest occupied n_z and is given by $n_{Fz} = [k_F L_z / \pi] \approx k_F L_z / \pi$, where $[x]$ indicates the integer part of x . The summation in Eq. (8) with $k_z = (\pi/L_z)n_z$ is evaluated analytically and is simplified by using Mathematica [18]; the electron density can be expressed as

$$\begin{aligned} n_e(z) = & \frac{k_F^2}{2\pi L_z} \left(n_{Fz} + \frac{1}{2} \right) - \frac{\pi}{12L_z^3} n_{Fz} (n_{Fz} + 1) (2n_{Fz} + 1) \\ & + \frac{1}{8\pi L_z^3} \left[(2n_{Fz} + 3)\pi^2 \cos\left(\frac{2(n_{Fz} + 1)\pi z}{L_z}\right) \csc^2\left(\frac{\pi z}{L_z}\right) \right. \\ & \left. + 2\left(\pi^2 (n_{Fz} + 1)^2 - k_F^2 L_z^2\right) \sin\left(\frac{(2n_{Fz} + 1)\pi z}{L_z}\right) \csc\left(\frac{\pi z}{L_z}\right) - \pi^2 \sin\left(\frac{(2n_{Fz} + 3)\pi z}{L_z}\right) \csc^3\left(\frac{\pi z}{L_z}\right) \right]. \quad (9) \end{aligned}$$

The total number of electrons is calculated using

$$\begin{aligned} \int_0^{L_z} n_e(z) dz = & \frac{1}{2\pi L_z} \sum_{n_z=1}^{n_{Fz}} (k_F^2 - k_z^2) \int_0^{L_z} dz \left[1 - \cos\left(2\frac{\pi}{L_z} n_z z\right) \right] \\ = & \frac{1}{2\pi L_z^2} \sum_{n_z=1}^{n_{Fz}} (k_F^2 L_z^2 - n_z^2 \pi^2) \quad (10) \end{aligned}$$

$$= \frac{k_F^2 n_{Fz}}{2\pi} - \frac{\pi}{12L_z^2} n_{Fz} (n_{Fz} + 1) (2n_{Fz} + 1). \quad (11)$$

Equation (11) is known. [15]

The total number of positive charges from ions is equal to the total number of free electrons denoted by N . The total number of positive charges N can be calculated by calculating a relation

for the total number of electrons, given by

$$2\frac{1}{4\pi}L_xL_y\sum_{n_z=1}^{n_{Fz}}(k_F^2 - k_z^2) = N, \quad (12)$$

which can be rewritten as [19]

$$\frac{L_xL_y n_{Fz}}{2\pi}\left[k_F^2 - \frac{1}{6L_z^2}(n_{Fz} + 1)(2n_{Fz} + 1)\pi^2\right] = N. \quad (13)$$

We find from Eq. (13) that

$$k_F^2 = \frac{\pi^2}{6L_z^2}(n_{Fz} + 1)(2n_{Fz} + 1) + \frac{2\pi N}{L_xL_y n_{Fz}}. \quad (14)$$

By substituting Eq. (14) into Eq. (11), we obtain

$$\frac{1}{L_z}\int_0^{L_z} dz n_e(z) = \frac{N}{L_xL_yL_z}. \quad (15)$$

The average positive charge density (denoted by ρ) should be given by the number of positive charges N averaged over the volume (given by $L_xL_yL_z$), *i.e.*, $\rho = N/(L_xL_yL_z)$. Equation (15) indicates that charge neutrality is satisfied; it is not necessary to introduce a new width for the ions instead of L_z to describe the shift of the jellium edge from the potential edge. Therefore, the jellium edge coincides with the potential edge.

The shift of the jellium edge from the potential edge follows from the following argument. If we loosely evaluate Eq. (8) by integration, we have [4, 17]

$$n_e^{(a)}(z) = \frac{L_z}{\pi}\frac{1}{2\pi L_z}\sum_{n_z=1}^{n_{Fz}}(k_F^2 - k_z^2)[1 - \cos(2k_z z)]\frac{\pi}{L_z} \quad (16)$$

$$\approx \frac{1}{2\pi^2}\int_0^{K_F} dk_z (K_F^2 - k_z^2)[1 - \cos(2k_z z)] \quad (17)$$

$$= \rho\left(1 + \frac{3\cos(2K_F z)}{(2K_F z)^2} - \frac{3\sin(2K_F z)}{(2K_F z)^3}\right), \quad (18)$$

where K_F appeared by evaluating k_F in the limit of $L_z \rightarrow \infty$, and $\rho = K_F^3/(3\pi^2)$ is given by Eq. (2). Similarly, we can loosely evaluate the average positive charge density by integration using Eq. (12): [4, 17]

$$\frac{1}{2\pi^2}L_xL_yL_z\int_0^{K_F} dk_z (K_F^2 - k_z^2) = \frac{K_F^3}{3\pi^2}L_xL_yL_z = N. \quad (19)$$

Therefore, the average positive charge density is given by $N/(L_xL_yL_z)$ and is obtained as ρ . We also find from Eq. (18)

$$\int_0^\infty dz [n_e^{(a)}(z) - \rho] = -\rho\frac{3\pi}{8K_F}. \quad (20)$$

If one notices that a single edge is present in the limit of $\pi/L_z \rightarrow 0$, the result suggests that the jellium edge is $3\pi/(8K_F)$ and is shifted inside from the potential edge to satisfy the charge neutrality condition; [4, 6–11] Equation (20) indicates $\int_0^{L_z} dz n_e^{(a)}(z) = \rho[L_z - (3\pi)/(8K_F)]$ when L_z is sufficiently larger than the Wigner-Seitz radius. The difference between the density calculated from the wave function and that calculated from the density of states is a mathematical consequence of taking the limit $\pi/L_z \rightarrow 0$. The difference disappears as long as we rigorously evaluate the quantized effect represented by summation, thus the difference is unphysical in thin slabs. We conclude that the jellium edge coincides with the potential edge for free electrons at least when the potential barrier along the z-direction is symmetric and infinite. Below, we show that the same conclusion can be reached for more general potentials.

We consider a slab of finite thickness L_z in the z-direction and extended infinitely in the x and y directions, where the Born-von Karman periodic boundary condition is imposed in x and y directions as before. The potential is zero at $0 \leq z \leq L_z$. A constant potential denoted by w_R is assumed for $L_z \leq z$, and a constant potential denoted by w_L is assumed for $z \leq 0$. The values of both w_R and w_L are assumed to be positive. The wave function is denoted by $\psi_n(z) \exp[i(k_x x + k_y y)] / \sqrt{L_x L_y}$, and the eigen-states are denoted by $n = 1, 2, \dots$. Because the eigen-states are orthonormal, the electron density can be written as

$$\begin{aligned} \int_{-\infty}^{\infty} dz n_e(z) &= \frac{1}{2\pi} \sum_{n_z=1}^{n_{Fz}} (k_F^2 - k_z^2) \int_{-\infty}^{\infty} dz |\psi_n(z)|^2 \\ &= \frac{1}{2\pi} \sum_{n_z=1}^{n_{Fz}} (k_F^2 - k_z^2). \end{aligned} \quad (21)$$

The total number of positive charges obeys Eq. (12) in the ground state. By combining Eq. (21) and Eq. (12), we obtain,

$$\frac{1}{L_z} \int_{-\infty}^{\infty} dz n_e(z) = \frac{N}{L_x L_y L_z}. \quad (22)$$

Equation (22) expresses the charge neutrality condition, where the positive charge density is obtained by averaging the total number of positive charges over the potential width denoted by L_z , yielding $\rho = N/(L_x L_y L_z)$. If the jellium edge differs from the potential edge, then L_z on the left-hand side of Eq. (22) must be changed. Therefore, we conclude that the jellium edge coincides with the potential edge.

III. CHEMICAL POTENTIAL RESULTS

By substituting the positive charge density given by $\rho = N/(L_x L_y L_z)$ into Eq. (14) and using the Wigner-Seitz radius given by $r_s = [3/(4\pi\rho)]^{1/3}$, we obtain a closed equation giving the thickness dependence of the Fermi wave vector as

$$k_F^2 = \frac{\pi^2}{6L_z^2}(n_{Fz} + 1)(2n_{Fz} + 1) + \frac{3}{2n_{Fz}} \frac{L_z}{r_s^3}. \quad (23)$$

where $n_{Fz} = [k_F L_z / \pi] \approx k_F L_z / \pi$. By introducing the approximation given by $n_{Fz} \approx k_F L_z / \pi$, we find

$$k_F = \frac{\pi}{4L_z} \left[1 + \frac{7\pi^{2/3}}{f(\ell_z)^{1/3}} + \frac{f(\ell_z)^{1/3}}{3\pi^{2/3}} \right] \quad (24)$$

$$\approx \left(\frac{9}{4} \pi \right)^{1/3} \frac{1}{r_s} + \frac{\pi}{4L_z} + \frac{7\pi^{5/3} r_s}{24 \times 18^{1/3} L_z^2}, \quad (25)$$

where $f(\ell_z) = 2^3 \times 3^5 \ell_z^3 + 81\pi^2 + 6 \sqrt{16 \times 3^8 \ell_z^6 + 4 \times 3^7 \ell_z^3 \pi^2 - 75\pi^4}$ and $\ell_z = L_z / r_s$. Apart from a constant in terms of L_z , the chemical potential of free electrons can be expressed as $\mu = \hbar^2 k_F^2 / (2m)$.

Consequently, the size dependence of the chemical potential can be rewritten as

$$\mu \approx \frac{\hbar^2}{2m} \left[\left(\frac{9}{4} \pi \right)^{1/3} \frac{1}{r_s} + \frac{\pi}{4L_z} + \frac{7\pi^{5/3} r_s}{24 \times 18^{1/3} L_z^2} \right]^2. \quad (26)$$

In the limit $L_z \rightarrow \infty$, we recover the bulk chemical potential expressed as [1]

$$\mu_b = \frac{\hbar^2}{2m} (3\pi^2 \rho)^{2/3} = \frac{\hbar^2}{2mr_s^2} \left(\frac{9\pi}{4} \right)^{2/3}. \quad (27)$$

In Fig 1, we show the chemical potential $\hbar^2 k_F^2 / (2m)$ of free electrons as a function of L_z calculated from Eq. (26). We also show the exact chemical potential obtained using Eq. (14) and $n_{Fz} = [k_F L_z / \pi]$. The figure is invariant under changes in the electron density, which indicates that the free electron model is characterized by a single length scale given by the Wigner-Seitz radius. Equation (26) indicates that the chemical potential is a monotonic decreasing function of L_z . The separation between quantum states increases by decreasing the thickness of the slab; the largest energy value of electrons in the ground state (μ) increases by increasing the separation between quantum states. This qualitative feature was already pointed out previously. [19, 20] The exact numerical result in Fig. 1 shows the oscillatory dependence on L_z . The oscillatory L_z dependence originates from the discreteness of the total number of free electrons. This result agrees with the oscillatory L_z dependence of the chemical potential reported previously. [5, 10, 19, 20]

In Fig. 2, we show the electron density profile given by Eq. (9) and a comparison with the electron density obtained from Eq. (18), where the limit $\pi/L_z \rightarrow 0$ is employed. The electron density is made dimensionless by multiplying it with r_s^3 . The figure is invariant under changes in the electron density. The result in Eq. (9) indicates that the electron density satisfies the boundary condition at $z = 0$ and $z = L_z$. The electron density in the middle of the thickness is higher than the average density because of the depletion of the electron density near the boundaries due to quantum confinement effect. By increasing the slab thickness, the difference between the average density and the density in the middle of the thickness decreases. When the positive charge density with the average electron density is uniformly distributed over the thickness determined by the potential edges, the electron density in the middle of the slab is higher than the positive charge density. If the positive charge density is assumed to be equal to the electron density in the middle of the thickness, the positive charge density should be distributed over the thickness narrower than that determined from the potential edges to maintain the overall charge neutrality in the slab. In this case, the positive charge density differs from the average electron density; as a result, the geometric edges differ from the potential edges. Both types of edges coincide when the positive charge density with the average electron density is uniformly distributed.

The electron density profile obtained from Eq. (9) shows oscillation with wavelength L_z/n_{Fz} . Using $n_{Fz} = [k_F L_z/\pi] \approx k_F L_z/\pi$, and Eq. (24) for k_F , the wavelength can be written as

$$\frac{L_z}{n_{Fz}} \approx k_F/\pi \approx \left(\frac{2\pi}{3}\right)^{2/3} r_s \approx 1.64r_s. \quad (28)$$

The oscillation shown in Fig. 2 is well characterized by the wavelength. If the bulk value of the Fermi wave vector obtained from Eq. (2) is introduced into Eq. (28), we find K_F/π . The result in Eq. (18) also shows oscillation with a wavelength given by K_F/π . However, it differs significantly from the exact result. The density of electrons obtained in the limit $\pi/L_z \rightarrow 0$ is lower than the exact result in the middle of the slab thickness. Moreover, we see that the approximate electron density does not fulfill the boundary condition at $z = L_z$. The electron density approaches zero only at $z = 0$.

Before closing this section, we comment on the energy required to excite an electron from the ground state. If we denote the right-hand side of Eq. (14) by $k_F^2(n_{Fz})$, the excitation energy can be

estimated from $\Delta\epsilon_F = \hbar^2/(2m)[k_F^2(n_{Fz} + 1) - k_F^2(n_{Fz})]$ as

$$\Delta\epsilon_F = \frac{\hbar^2}{12mL_z^2} \left(\pi^2 (5 + 4n_{Fz}) - \frac{9(L_z/r_s)^3}{n_{Fz}(n_{Fz} + 1)} \right) \quad (29)$$

$$= \frac{\pi^2 \hbar^2}{mL_z^2} \left(1 - \frac{1}{3} \frac{K_F^2 r_s^3}{L_z} \right), \quad (30)$$

where Eq. (25) is used. For sodium, $\Delta\epsilon_F$ is estimated to be about 0.026 (eV) when the slab thickness is 5.3 (nm) using Eq. (30). If the Wigner-Seitz radius is given by $r_s = 3$ (Bohr), $\Delta\epsilon_F$ is also about 0.026 (eV) when the slab thickness is 5.3 (nm). The results suggest the length scale of the Kubo effect at room temperature; the quantization of one electronic level at the Fermi level results in remarkable effects in thermodynamic properties of fine metals. [21] Equation (30) indicates that the Kubo effect can be observed for the thicker metal slabs if the temperature is lowered from room temperature.

IV. SURFACE ENERGY RESULTS

Similarly, we can calculate the surface energy. First, we express the total energy as [19]

$$E_t = \frac{\hbar^2}{2m} \frac{2L_x L_y}{(2\pi)^2} \sum_{n_z=1}^{n_{Fz}} \int_0^{\sqrt{k_F^2 - k_z^2}} dk_{\parallel} 2\pi k_{\parallel} (k_{\parallel}^2 + k_z^2) \quad (31)$$

$$= \frac{\hbar^2}{2m} \frac{L_x L_y}{4\pi} \sum_{n_z=1}^{n_{Fz}} (k_F^4 - k_z^4) \quad (32)$$

$$= \frac{\hbar^2}{2m} \frac{L_x L_y}{4\pi} \left[n_{Fz} k_F^4 - \frac{\pi^4}{30L_z^4} n_{Fz}(n_{Fz} + 1)(2n_{Fz} + 1)(3n_{Fz}^2 + 3n_{Fz} - 1) \right], \quad (33)$$

where k_z is given by Eq. (5). Then, we decompose the total energy into the bulk energy per unit volume and the two parts of the surface energy per unit area of the slab as [19]

$$E_t = \epsilon_b L_x L_y L_z + 2\epsilon_s L_x L_y, \quad (34)$$

where the bulk energy is obtained using $n_{Fz} \approx k_F L_z / \pi$ as

$$\epsilon_b = \lim_{L_z \rightarrow \infty} \frac{E_t}{L_x L_y L_z} \quad (35)$$

$$= \frac{\hbar^2 K_F^5}{10m\pi^2}, \quad (36)$$

where k_F is replaced with K_F since the bulk energy can be obtained in the limit of $L_z \rightarrow \infty$. The obtained bulk energy is equal to the total energy given by $(3N/5)\hbar^2 K_F^2/(2m)$ divided by $L_x L_y L_z$ as

it should be. [1] Now, we calculate the surface energy. The surface energy is obtained from Eq. (33) using the decomposition given by Eq. (34) as

$$\frac{\epsilon_s}{\epsilon_{s0}} = 2 \left(\frac{4}{9\pi} \right)^{4/3} \left[n_{Fz} (k_F r_s)^4 - \frac{\pi^4 r_s^4}{30 L_z^4} n_{Fz} (n_{Fz} + 1) (2n_{Fz} + 1) (3n_{Fz}^2 + 3n_{Fz} - 1) \right] - \frac{8}{5\pi} K_F L_z \quad (37)$$

$$\approx 1 + \frac{\pi}{2K_F L_z} - \frac{\pi^2}{24(K_F L_z)^2}, \quad (38)$$

where the surface energy in the limit of $L_z \rightarrow \infty$ is given by

$$\epsilon_{s0} = \frac{1}{32\pi} \frac{\hbar^2 K_F^4}{m}. \quad (39)$$

Equation (39) was obtained earlier. [22]

In Fig. 3, we compare the surface energy given by Eq. (39) with the experimental values. The metal species are chosen so that the Sommerfeld parameter of the heat capacity is close to that estimated from the free electron model. Specifically, the criterion is that the ratio of the measured to the free electron values of the Sommerfeld parameter is between 0.7 and 1.3. The solid line is the surface energy calculated from the free electron model of the slab obtained from Eq. (39). Compared to the Sommerfeld parameter, the larger deviation of the experimental values from the theoretical results of the free electron model is found for the surface energy of the slab. The deviation could originate from the oversimplification in the free electron model of the slab, where the inhomogeneity in the background positive charges in particular near the surface is ignored. Though we did not consider finite barriers, the effect of finite barrier height can be taken into account in a straightforward manner as sketched in Theory section and can be ignored as long as the lowest barrier height sufficiently exceeds the chemical potential. In the same figure, we show the known result given by $\epsilon_{s0} \approx \hbar^2 K_F^4 / (160\pi m)$ which is derived by applying the charge neutrality condition using an average positive charge density that is different from the expression presented here. [9, 17] We consider the free electron model of the slab; the surface energy is calculated from the natural decomposition of the total energy into the bulk part and the surface parts. Then, the summation appeared due to quantization in the direction of the slab thickness is rigorously evaluated. The deviation introduced by approximating the summation by integration is well captured in the electron density shown in Fig. 2. As a result, the dashed line significantly differs from the solid line in Fig. 3.

In Fig. 4, we show the surface energy as a function of L_z calculated from Eq. (37). The surface energy is normalized by that taking the limit $L_z \rightarrow \infty$. We also show the surface energy by taking

into account the discreteness of the total number of free electrons. By substituting k_F obtained from Eq. (23) into Eq. (37) using $n_{Fz} = [k_F L_z / \pi]$, we obtained the exact result of the surface energy. The figure is invariant under changes in the electron density. Equation (38) indicates that the surface energy is a monotonic decreasing function of L_z like the chemical potential. The exact numerical result in Fig. 4 shows the oscillatory dependence on L_z . The oscillatory L_z dependence originates from the discreteness of the total number of free electrons as in the case of the chemical potential.

V. CONCLUSION

We have considered the electron density and the number of positive charges by rigorously taking into account the quantum effect while keeping the discrete sum in the free electron model for a thin metal slab. We showed that the jellium edge coincides with the rectangular potential edge. The effect of quantum confinement on the chemical potential and surface energy in a thin slab was subsequently studied. The thickness dependence of the chemical potential was derived as Eq. (26); the chemical potential (Fermi energy) increases as the thickness of the slab decreases because the separation between quantized states becomes wider. The thickness dependence of the surface energy was derived as Eq. (38) and showed the similar dependence on the thickness of the slab. More accurate results for the chemical potential and surface energy that reflect the discrete nature of the number of electrons in the Wigner-Seitz cell showed the oscillatory thickness dependence superimposed on top of the continuous thickness dependence mentioned above.

In our analysis, quantized effects due to confinement of electrons in a thin slab were considered according to the free electron model, where the length scale is characterized by the Wigner-Seitz radius. Lattice structures and lattice constants could affect the physical quantities as the slab thickness decreases. A full quantitative characterization of a particular metal film based on the aforementioned structure is beyond the scope of the present study. The electrostatic interaction, the exchange interaction and the correlation interaction were also ignored. Nevertheless, we qualitatively discussed the quantum size effect on the chemical potential and the surface energy in a thin metal slab. In some theories, [4–6, 8, 10, 11] the shift of the jellium edge from the potential edge was calculated, and the chemical potential was affected by the shift. We showed that such a shift is unnecessary if both the electron density and the total number of positive charges are evaluated by taking into account the finite width of the metal slab. By using the charge neutrality condition

together with the rigorous results for the average positive charge density and the electron density profile, we showed that the jellium edge indeed coincides with the potential edge.

- [1] C. Kittel and H. Kroemer, *Thermal Physics* (W. H. Freeman, 1980).
- [2] N. D. Lang and W. Kohn, *Phys. Rev. B* **1**, 4555 (1970).
- [3] R. Stratton, *Phys. Lett.* **19**, 556 (1965).
- [4] A. Kiejna and K. Wojciechowski, *Metal Surface Electron Physics* (Pergamon, Oxford, 1996).
- [5] P. P. Kostrobij and B. M. Markovych, ArXiv e-prints (2018), arXiv:1804.08884 [cond-mat.stat-mech].
- [6] F. Schulte, *Surf. Sci.* **55**, 427 (1976).
- [7] J. Bardeen, *Phys. Rev.* **49**, 653 (1936).
- [8] J. E. van Himbergen and R. Silbey, *Phys. Rev. B* **18**, 2674 (1978).
- [9] H. B. Huntington, *Phys. Rev.* **81**, 1035 (1951).
- [10] P. P. Kostrobij and B. M. Markovych, *Phys. Rev. B* **92**, 075441 (2015).
- [11] Y. Han and D.-J. Liu, *Phys. Rev. B* **80**, 155404 (2009).
- [12] V. D. Dymnikov, *Phys. Solid State* **53**, 901 (2011).
- [13] A. Paskin and A. D. Singh, *Phys. Rev.* **140**, A1965 (1965).
- [14] B. Smith, *Phys. Lett.* **18**, 210 (1965).
- [15] C. Thompson and J. Blatt, *Phys. Lett.* **5**, 6 (1963).
- [16] B. Wu and Z. Zhang, *Phys. Rev. B* **77**, 035410 (2008).
- [17] A. Sugiyama, *J. Phys. Soc. Jpn.* **15**, 965 (1960).
- [18] Wolfram Research, Inc., *Mathematica, Version 11.3* (Champaign, IL, 2018).
- [19] P. Czoschke, H. Hong, L. Basile, and T.-C. Chiang, *Phys. Rev. B* **72**, 075402 (2005).
- [20] A. V. Korotun, *Phys. Solid State* **57**, 391 (2015).
- [21] R. Kubo, *J. Phys. Soc. Jpn.* **17**, 975 (1962).
- [22] J. Waber, E. Kennard, and Y.-P. Tsui, *J. Phys. Colloques* **33**, C3 (1972).

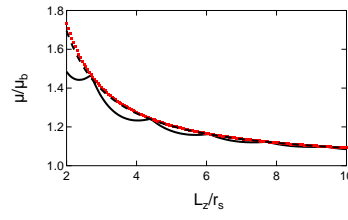


FIG. 1. (Color online) Normalized chemical potential is shown against the thickness of the slab. The thickness of the slab is normalized by the Wigner-Seitz radius given by $r_s = [3/(4\pi\rho)]^{1/3}$. The dashed line is calculated using Eq. (24) and normalized by the bulk value given by μ_b [Eq. (27)]. The (red) dots are calculated from Eq. (26). The solid line indicates the exact result shown in the main text.

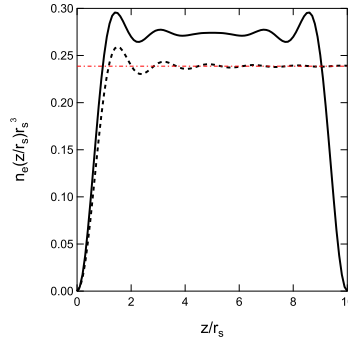


FIG. 2. (Color online) The electron density is shown as a function of distance from the surface when $L_z = 10r_s$. The electron density is made dimensionless by multiplying it with r_s^3 . Both the electron density and the distance from the surface of the slab are normalized by the Wigner-Seitz radius $r_s = [3/(4\pi\rho)]^{1/3}$. The solid line shows the exact result obtained from Eq. (9). The normalized average density is shown by the (red) dashed-dotted line, which is given by $3/(4\pi)$ because $\rho = 3/(4\pi r_s^3)$. The dashed line shows the result from Eq. (18) obtained in the limit $\pi/L_z \rightarrow 0$.

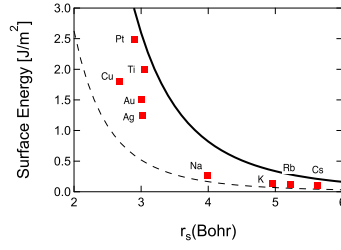


FIG. 3. (Color online) The surface energy is shown against the Wigner-Seitz radius. The solid line is obtained from Eq. (39) and the dashed line indicates the classical result of $\hbar^2 k_F^4 / (160\pi m)$. The (red) dots indicate the experimental values of the surface energies of metals.

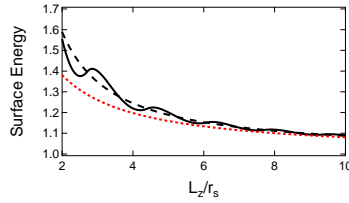


FIG. 4. (Color online) Normalized surface energy is shown against the thickness of the slab. The thickness of the slab is normalized by the Wigner-Seitz radius given by $r_s = [3/(4\pi\rho)]^{1/3}$. The dashed line is calculated from Eq. (37) with $n_{Fz} \approx k_F L_z / \pi$ and normalized by the bulk value of the surface energy [Eq. (39)]. The (red) dots are calculated from Eq. (38). The solid line indicates the exact result obtained from Eq. (37) and Eq. (23) using $n_{Fz} = [k_F L_z / \pi]$.